

Multi-Dimensional Vector ISA Extension for Mobile In-Cache Computing

Alireza Khadem[†], Daichi Fujiki[‡], Hilbert Chen[†], Yufeng Gu[†], Nishil Talati[†], Scott Mahlke[†], and Reetuparna Das[†]

University of Michigan[†], Institute of Science Tokyo[‡]

{arkhadem,cyaa,yufenggu,talatin,mahlke,reetudas}@umich.edu, dfujiki@artic.iir.isct.ac.jp

Abstract—In-cache computing technology transforms existing caches into long-vector compute units and offers low-cost alternatives to building expensive vector engines for mobile CPUs. Unfortunately, existing long-vector Instruction Set Architecture (ISA) extensions, such as RISC-V Vector Extension (RVV) and Arm Scalable Vector Extension (SVE), provide only one-dimensional strided and random memory accesses. While this is sufficient for typical vector engines, it fails to effectively utilize the large Single Instruction, Multiple Data (SIMD) widths of in-cache vector engines. This is because mobile data-parallel kernels expose limited parallelism across a single dimension.

Based on our analysis of mobile vector kernels, we introduce a long-vector **Multi-dimensional Vector ISA Extension (MVE)** for mobile in-cache computing. MVE achieves high SIMD resource utilization and enables flexible programming by abstracting cache geometry and data layout. The proposed ISA features multi-dimensional strided and random memory accesses and efficient dimension-level masked execution to encode parallelism across multiple dimensions. Using a wide range of data-parallel mobile workloads, we demonstrate that MVE offers significant performance and energy reduction benefits of $2.9\times$ and $8.8\times$, on average, compared to the SIMD units of a commercial mobile processor, at an area overhead of 3.6%.

I. INTRODUCTION

Data-parallel kernels are ubiquitous in various mobile application domains, from operating systems (*e.g.*, Android) to web applications (*e.g.*, Google Chrome) [49]. These kernels typically consist of tight loops that interleave scalar and vector processing. Single Instruction Multiple Data (SIMD) pipelines integrated with a CPU core are employed to exploit these applications' *fine-grain data-level parallelism*. SIMD execution amortizes the cost of instruction fetch and decode to improve the performance and energy consumption of data-parallel applications, *i.e.*, two primary concerns of resource-limited mobile devices.

While mobile applications benefit from vector architectures, scaling up vector register files and ALUs incurs significant area and power overheads to the mobile processors. Hence, all Arm mobile processor implementations are restricted to 128-bit vector units. Alternatively, various In-SRAM computing schemes [8]–[10], [31], [46], [87] repurpose cache arrays to build high-throughput and power-efficient vector engines

with minimal area overhead. For instance, half the size of a small private L2 cache (256 KB) in a mobile CPU can be transformed into an 8192-lane bit-serial vector engine with a 3.5% area overhead [35] to the die. The cache SRAM arrays provide compute capability and also act as vector registers. Furthermore, they function as regular caches without performance overhead when not used for In-SRAM computing.

Existing long-vector ISA extensions (*e.g.*, RISC-V RVV [5] and Arm SVE [80]) provide one-dimensional strided and random memory accesses. While sufficient for typical vector engines (128–1024 bits), these fall short of effectively utilizing long-vector in-cache vector engines with large SIMD width (8192×32 bits). Using conventional long-vector ISAs with only one-dimensional memory accesses requires several vector manipulation instructions to load/store and unpack/pack multiple dimensions of the data structures to a single long-vector register. This substantially increases the instruction count and core-cache communication, under-utilizing the in-cache SIMD lanes.

This issue is compounded by the fact that mobile vector kernels expose *limited one-dimensional (1D) parallelism*. Our evaluation shows an average of 635 1D parallelism in a vector benchmark suite for mobile processors [49]. This benchmark encompasses mobile applications from various domains, such as Chromium [2] (browser and OS), Android [1] (OS), PDFium [4] (PDF rendering engine), and WebRTC [6] (real-time voice/text/video communication APIs for conferencing platforms such as Zoom, Microsoft Teams, Slack, or Google Meet). For example, the audio processing module of the WebRTC (*webaudio* [37]) simultaneously processes multiple audio chunks, each containing different channels of 128 audio samples, which limits the 1D parallelism to only 128 elements.

This observation motivates MVE, a long-vector **Multi-dimensional Vector ISA Extension** for mobile in-cache computing. The proposed ISA provides multi-dimensional strided and random memory accesses, as well as efficient dimension-level masked execution. This flexible instruction set increases the Data Level Parallelism (DLP) exposed to the in-cache vector engine to multiple dimensions of the mobile kernels. A higher DLP allows utilizing all 8192 in-cache SIMD compute lanes with few vector instructions.

To realize the proposed MVE ISA, we design a compute-capable cache architecture that targets small private L2 caches for a tight integration with the core. The proposed architecture

©2025 IEEE. Personal use of this material is permitted. Permission from IEEE must be obtained for all other uses, in any current or future media, including reprinting/republishing this material for advertising or promotional purposes, creating new collective works, for resale or redistribution to servers or lists, or reuse of any copyrighted component of this work in other works.

leverages fine-grain communication between the core and L2 cache to interleave scalar and vector instructions between the scalar core and the in-cache vector engine. Hence, MVE provides an alternative way of scaling vector units for processing fine-grain data-parallel mobile kernels.

This paper offers the following contributions:

- We propose a long-vector ISA extension that encodes parallelism across multiple dimensions using multi-dimensional strided and random memory accesses and efficient dimension-level masking. Compared to RISC-V RVV [5], this instruction set improves the in-cache vector engine utilization from 23% to 60% and enhances the performance by $3.8\times$, on average.
- We design cache architecture for multi-dimensional vector ISA. We analyze and evaluate different In-SRAM computing schemes for the proposed architecture, including bit-serial [31], bit-parallel [9], bit-hybrid [10], and associative computing [19].
- We validate the effectiveness of our solutions on twelve real-world mobile libraries [49]. An end-to-end system design with a long-vector bit-serial in-cache computing model improves the performance and energy of commercial vector CPUs by $2.9\times$ and $8.8\times$.
- We compare MVE in-cache vector processing to a mobile GPU. Our measurements show that domain-specific accelerators (GPUs and DSPs) suffer from the kernel launch and data copy overhead. This is crucial for the fine-grain data parallelism, which benefits from a long-vector engine tightly integrated with the core.
- We analyze and find that coarse-grain Single-Instruction Multiple-Thread (SIMT) models proposed for server class in-cache computing (e.g. Duality Cache [35]) are inefficient for mobile kernels due to the high compute latency and numerous register spills and fills.

II. BACKGROUND

A. Long Vector Processing

Long-vector ISA Extensions. Table I compares the state-of-the-art long-vector ISA extensions, *i.e.*, RISC-V vector extension (RVV) [5], Arm Scalable Vector Extension (SVE) [80], and NEC [53]. SVE and NEC support up to 2K bit and 16K bit vector lengths. Using SVE and NEC for the in-cache long-vector engine requires numerous instructions to target all 8K 32 bit SIMD lanes, increasing the core-cache communication.

RVV supports 1D strided vector accesses. NEC provides 2D strided loads and stores restricted to a constant 16×16 input matrix size. An efficient long-vector ISA extension tailored for the small 1D DLP of mobile applications requires *multi-dimensional* and *flexible* strided memory accesses.

RVV offers random memory accesses from a base address and predetermined offsets stored in an index vector register. SVE supports both the random base and random offset accesses. These instructions are not efficient for capturing the random memory accesses in mobile kernels, which often have multiple unique base addresses in the highest dimension, followed by strided patterns for lower dimensions.

TABLE I
VECTOR ISA EXTENSION COMPARISON

Feature	MVE (This Work)	RISC-V RVV [5]	Arm SVE [80]	NEC [53]
Max Vector Length	infinite	infinite	2048 bits	16384 bits
Strided Access	Flexible 4D	Flexible 1D	-	Constant 2D
Random Access	Random Base + Strided Offset	Random Offset	Random Base / Random Offset	-
Masked Execution	Predicate / Dimension-Level	Predicate	Predicate	Predicate

Finally, all three long-vector ISA extensions support predicated execution for irregular DLP patterns. However, generating predicate masks with scalar or long-latency in-cache vector instructions for 8K SIMD lanes is expensive. We introduce a coarse-grain dimension-level masking approach for the multidimensional access patterns.

Long-vector Engines are designed and fabricated by both the industry [22], [27], [53], [74], [77], [78] and academia [15], [20], [62], [63], [68], [75]. These units are mostly employed by the supercomputers with abundant area and power resources. For example, Vitruvius+ [63] is an RVV-based coprocessor which has 16K bit vector registers. The vector units though have 8 dual-precision or 16 single-precision SIMD lanes. Each instruction is scheduled on the SIMD lanes in 64 cycles in a vector manner. This coprocessor requires an area of $1.3mm^2$ at a 22nm technology ($\sim 0.4mm^2$ at 7nm) which is significant compared to the evaluated Arm Cortex-A76 core ($\sim 1.2mm^2$ at 7nm), including two 128-bit Neon ASIMD units and private L1 and L2 caches.

Due to the high area overhead of long-vector engines, all Arm application processors employ 128-bit ASIMD units since the introduction of Arm Neon technology. MVE utilizes the untapped private L2 cache resources and re-purposes them to $8K\times 32$ bits in-cache bit-serial SIMD lanes private to each core with 3.6% area overhead to the core.

B. In-Cache Computing

In-Cache computing [8], [31], [34], [47], [48] repurposes cache SRAM arrays to SIMD units. Figure 1(a) shows a mobile core with half of the L2 cache repurposed for in-cache computing. Neural Cache [31], which we build upon, proposes data elements are vertically aligned to the SRAM bitlines. SRAM peripherals compute bit-serial operations in-parallel for all data elements, as shown in Figure 1(b). Therefore, a SRAM array with 256 bitlines provides 256 SIMD lanes, and a 256KB L2 cache slice with 32 SRAM arrays can embody an 8192-lane bit-serial vector engine. In this section, we describe the architecture of prior In-SRAM computing schemes:

(a) **Bit-Serial Computing (BS)** [31] vertically aligns the array elements in the bitlines. By activating two word-lines of an SRAM array, Sense Amplifiers (SA) at the peripheral logic calculate the logical AND and NOR of a bit-slice across all elements of two input arrays. Extra logic is employed (blue components of Figure 1(c)) to compute the NAND, OR, and XOR of bit-slices. An n -bit integer addition is performed

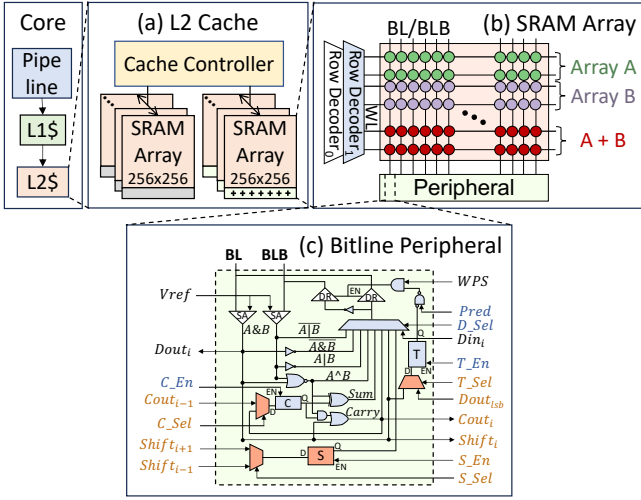


Fig. 1. (a) Mobile core with in-cache computing enabled for half of the L2 cache. (b) In-SRAM computing activates two word-lines of an SRAM array using an extra row decoder. (c) Bit-Serial (blue), Bit-Hybrid, and Bit-Parallel (blue + orange) modifications to the bitline peripheral.

in n cycles using additional logic to compute the sum and carry-out. A Carry latch (C) stores the carry-out in the bitline peripheral as the carry-in of the next bit. A two's complement subtraction is computed in $2n$ cycles by negating B and adding A and \bar{B} using the carry-in (C) set to 1. Integer multiplication requires $n^2 + 5n$ cycles. First, each i^{th} bit of the multiplicand is stored in the Tag latch (T) as an enabling signal to the bitline drivers. Next, the multiplier is conditionally added to the results, starting from the i^{th} bit. Constant shift operation is supported in n cycles by reading input bit-slices and writing to bit-slices of the shifted result, offset by the defined shift value. Variable shift needs $\mathcal{O}(n \log n)$ cycles [35] to read each i^{th} bit of B to the T latch and perform conditional constant shift with 2^i bit value. Duality Cache [35] extends these integer operations to floating-point arithmetic operations.

(b) **Bit-Parallel [9] (BP) and Bit-Hybrid [10] (BH).** BS maximizes parallelism to 8K SIMD lanes but has high arithmetic latency. VRAM [9] introduces BP, aligning n -bit data horizontally in a word-line. This reduces parallelism to $8K/n$ SIMD lanes yet improves latency by a factor of n . EVE [10] introduces BH by merging BS and BP schemes to balance the latency and parallelism. BH splits n -bit data into p -bit segments where segments are computed using BP, and combined using BS. BP and BH computing require communication across bitline peripherals which incurs area and frequency overheads [9]. Figure 1(c) shows the additional logic for the inter-bitline communication in orange. EVE [10] employs Manchester carry chain and routes carry-out to the next bitline for the full addition inside a segment while the C flip-flop is used for the addition between segments.

(c) **Associative Computing (AC) [19].** In contrast to the prior schemes, AC does not employ extra logic in the bitline peripheral for logical operations. Instead, AC employs the search and update operations of the Binary Content Addressable Memory (BCAM) structures [46]. To perform any logical operation, AC executes a search and update for each row of

the truth table. Using AC, CAPE [19] horizontally aligns a bit-slice of all array elements in a word-line. Since CAPE distributes different bit-slices in different SRAM arrays, it executes a bit-wise operation in parallel for all bits in $\mathcal{O}(1)$ cycles. Prior work [18] exploits the low latency of these bit-wise logical operations to accelerate database workloads. However, the search and update operations are performed sequentially for different bits of full addition, since it requires carry propagation between bit slices. An n -bit integer subtraction/addition requires $8n + 2$ cycles. Because other arithmetic operations are decomposed to addition and subtraction, they incur high operation latency as well.

In **summary**, all In-SRAM computing schemes convert the cache SRAM arrays to a high-throughput long-vector engine. Therefore, MVE is required to utilize the multi-dimensional DLP of mobile kernels for the numerous in-cache SIMD lanes. While Section VII-B evaluates this claim, we use the bit-serial computing to explain our contributions throughout this paper.

III. INSTRUCTION SET ARCHITECTURE

We draw on the insights from analyzing Swan [49], a state-of-the-art benchmark suite of data-parallel applications for mobile processors. We find that multidimensional data structures are prevalent in mobile applications. These insights inform our design choices, allowing us to effectively exploit mobile workload characteristics in the proposed MVE extension.

A. Design Goals

Given the high throughput of the in-cache computing engine, the *key ISA design challenge* is to achieve high compute resource utilization by developing a *compact ISA* that expresses vector computation in few instructions. An ISA that generates numerous dynamic instructions leads to instruction issue bottlenecks and overflows the micro-architecture modules. Consequently, the scalar core cannot issue sufficient instructions to keep in-cache vector units busy.

In addition, prior in-cache ISA extensions [8], [54], [79] expose the cache geometry and data layout to programmers, requiring them to load and align data elements along specific SRAM bitlines to ensure operand locality. This approach increases programming complexity, as programmers must deal with cache bank, set, way, word-line, and bitline coordinates, resulting in binaries incompatible with other cache architectures. In contrast, we aim to abstract away these complexities by presenting in-cache computing as a long-vector processing engine. Programmers can use in-cache vector instructions and registers similar to other long-vector extensions, while the underlying architecture transparently maps long-vector registers to SRAM bitlines and word-line coordinates.

B. Physical Register Abstraction.

Figure 2 shows the data layout of vector registers in the cache: (a) MVE supports N Physical Registers (PR_0 to PR_{N-1}). (b) Internally, data elements of a physical register are transposed and placed vertically in a bitline to support bit-serial In-SRAM operations. Thus, an SRAM array with 256

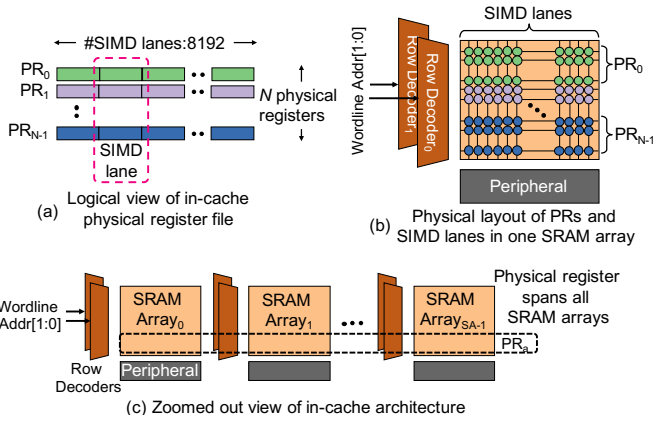


Fig. 2. (a) MVE operates on N long-vector in-cache registers. (b) In-cache data elements and SIMD lanes use the vertical data layout of bit-lines. (c) An in-cache physical register spans all compute-capable SRAM arrays.

bitlines provides 256 data elements for a PR. (c) Each PR spans across all SRAM arrays. Therefore, an in-cache long-vector PR contains 8K data elements using 32 SRAM arrays.

We observe that the mobile data-parallel kernels of the Swan benchmark suite [49] operate on multi-dimensional data structures using nested loops and utilize at most four dimensions. Further, mobile data-parallel kernels often operate on small input data sizes, so one dimension is insufficient to harness the throughput of in-cache vector engines. Thus, rather than addressing each of 8K SIMD lanes in a linear address space (*i.e.*, $PR_i[s]$), MVE ISA treats physical registers as multi-dimensional logical registers (*i.e.*, $PR_i[w][z][y][x]$).

MVE cache controller (Section V) maintains the vector engine configurations in specific *Control Registers (CR)*. Programmers select the dimension count and lengths using config instructions that set the CRs. Logical register indices are flattened-out to the 8K SIMD lanes and mapped to a *MVE physical register* by the MVE controller. Many kernels use the same memory access pattern for multiple input batches. Therefore, the overhead of configuring CRs is amortized over multiple vector executions.

The physical vector register file in the conventional vector architectures has a fixed number of registers with a constant width, such as 40 16K bit registers in the Vitruvius+ [63] architecture. Vector ISA extensions, like RVV [5], offer a constant number of registers but vary the vector length based on the data precision. In contrast, the bit-serial layout of the In-SRAM computing offers a constant vector length (8K bitlines) but allows a variable number of registers based on the data widths. While a fixed vector length regardless of the data precision simplifies the vectorization, a variable number of registers complicates register allocation (Section III-G).

MVE compute instructions perform the same operation on all SIMD lanes of the physical register, yet loads and stores to the physical registers can target different memory locations. As we discuss next, the multi-dimensional logical vector register abstraction allows offloading versatile and multi-dimensional memory access patterns.

C. Strided Memory Access with Possible Replication

The memory access of data-parallel kernels follows a regular pattern: nested loops process multiple data dimensions, and the base memory address of each iteration differs with a constant stride. Therefore, we propose multi-dimensional strided memory access instructions as shown in Algorithm 1.

Algorithm 1 Strided Multi-dimensional Vector Load

Input: $Dim_{[3:0]}$.Length : CRs, Base Address, and $S_{[3:0]}$: Strides

- 1: **for** w in $[0 : Dim_3.Length)$ **do**
- 2: **for** z in $[0 : Dim_2.Length)$ **do**
- 3: **for** y in $[0 : Dim_1.Length)$ **do**
- 4: **for** x in $[0 : Dim_0.Length)$ **do**
- 5: $PR_i[w][z][y][x] = MEM[Base + w \times S_3 + z \times S_2 + y \times S_1 + x \times S_0]$

As an example, a typical pattern employed in the *Intrapicture Prediction* kernel of image and video coding [83] is shown in Figure 3. This kernel needs a 3D strided vector load with $S_0 = 1$, $S_1 = 0$, and $S_2 = 3$. The input data is located in a 2D data structure but is loaded into a 3D logical register for the actual computation. The strided vector load instruction encodes data loading from 2D to 3D along with the replication in a single instruction. The stride $S_1 = 0$ facilitates the replication of each element in an input data row to an entire column in the 3D logical register. The figure further shows a flattened-out data mapping from a 3D logical register representation to different SIMD lanes of a physical register.

1D vector ISA extensions like RVV [5] would employ 6 strided load instructions to access each row of the input data (*e.g.*, $[0][1][2]$) separately to a 3-element segment of the vector register, while masking off the other segments. Further scalar instructions are needed to compute the mask and 6 instructions to load them. MVE encodes this pattern in a single instruction without needing any masks.

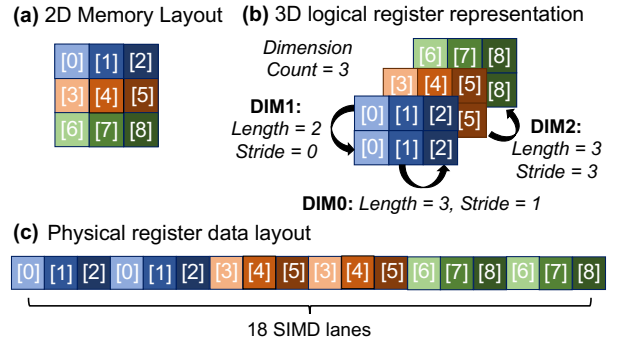


Fig. 3. Strided memory access example of *Intrapicture Prediction* kernel: loading from (a) 2D memory layout to (b) 3D logical registers, mapped to (c) the SIMD lanes of flattened-out physical registers by MVE controller.

Each stride value (S_i) takes up to 16 instruction bits. Encoding multiple stride values for different dimensions increases the instruction width. However, our analysis shows that stride values of 0 (for replication) and 1 (for sequential access) are frequently used. Thus, instead of a 16-bit absolute stride value, we encode a 2-bit *stride mode* for each dimension (8 bits for four dimensions). Modes 0 and 1 encode frequently-used

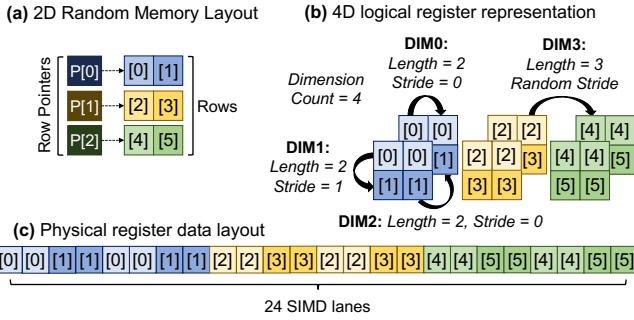


Fig. 4. Random memory access of $h2v2$ Upsample kernel: loading from (a) random row pointers to (b) 4D logical registers. (c) shows the SIMD lanes of the flattened-out physical registers.

stride values of 0 and 1. *Mode 2* is designed for the sequential accesses, where the stride in the higher dimensions differs. For example, when loading from a row-wise 2D matrix, the stride value of the row dimension equals to the number of columns. Therefore, using mode 2 for the i^{th} dimension provides a stride of $S_i = S_{i-1} \times \text{Dim}_{i-1}.\text{Length}$. If the desired stride value is neither of the mentioned modes, we provision a load and a store stride CR for each dimension in MVE controller, which is set by the config instructions. *Mode 3* uses these CR values.

D. Random Memory Access with Striding and Replication

We observe that in some mobile data-parallel kernels, the outer-most loop (highest dimension) requires unique base addresses, while the inner loops follow the stride pattern. Figure 4 demonstrates this concept with an example of *libjpeg* library [57]. *libjpeg* allocates rows in separate memory locations. $h2v2$ Upsample kernel replicates each pixel horizontally and vertically into 4 pixels. While the address in the 4th dimension is random (row pointers), other dimensions follow the stride values of 0 (replicate vertically), 1 (row pixels), and 0 (replicate horizontally).

The random memory access instruction of MVE encodes the address of the input pointer array. MVE controller fetches the random base addresses from this array, and employs stride values for the inner dimensions as shown in Algorithm 1.

$$PR_i[w][z][y][x] = MEM[Base_w + z \times S_3 + y \times S_2 + x \times S_1] \quad (1)$$

RVV [5] supports a single base address with random offsets located in a vector register. Implementing the above memory access pattern with these instructions requires 3 masked random memory accesses per base address, scalar instructions to compute mask, and 6 extra memory accesses to load the mask and offset vector registers. In contrast, MVE encodes this pattern in a single random memory access without scalar instruction overhead.

E. Efficient Masked Execution

MVE supports masked execution using two types of instructions: (a) *Conventional Predictated Execution*: MVE provides compare operations whose result are stored in the Tag Latch (T) to mask off each SIMD bit-line independently (leaves of dimension tree in Figure 5). (b) *Dimension-Level Mask Operations*: We observe that most of the data-parallel kernels

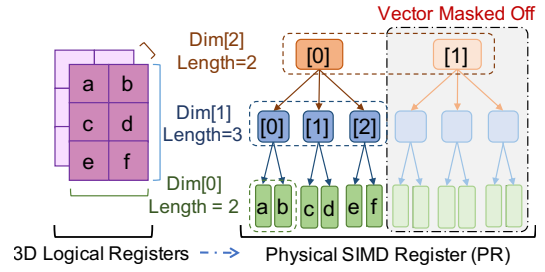


Fig. 5. MVE Controller maps multi-dimensional *logical registers* to 1D *Physical SIMD Registers*. Efficient dimension-level masked execution masks off leaves under a node in the highest dimension of the tree (iterations of the outer-most loop).

require *coarse-grain* masked execution where SIMD lanes corresponding to the outermost loop are masked off (leaves under the orange node [1]). We keep a mask CR that contains one bit for each element of the highest dimension. We set the maximum length of the highest dimension to 256 to limit the mask CR size. Mask values are calculated by the scalar instructions and set in the MVE controller using vector mask instructions, that mask on/off SIMD lanes of a specific element of the highest dimension. Using conventional predicated execution to implement this semantic requires computing the mask value of each element in the scalar core, storing them to the memory, and loading them to a vector mask register. Dimension-level mask operations are efficient as they do not use In-SRAM physical registers or scalar instructions.

F. Programming Model

MVE supports 8/16/32/64-bit un/signed integer and 16/32-bit floating-point data types denoted by $b/w/dw/qw$ and hf/h suffixes. 29 operations are implemented for each data type, which are classified in Table II. *Config* operations set the CRs of the MVE controller and are not executed on SRAM arrays. *Move* operations convert and copy registers. *Load* and *Store* operations provide both strided and random vector memory accesses. *Arithmetic* operations are used to set the value of a register based on source registers and immediate values.

TABLE II
MVE INSTRUCTIONS

Type	Operation	Assembly	BS Latency*
Config	set dim count	<code>vsetdimc rs</code>	-
	set dim length	<code>vsetdiml rs1 rs2</code>	
	(un)set mask	<code>v(un)setmask rs</code>	
	set kernel width	<code>vsetwidth imm8</code>	
Move	convert	<code>vcvt vd vs</code>	n
	copy	<code>vcpy vd vs</code>	
Memory Access	strided load	<code>vslld vd rs1 rs2</code>	-
	random load	<code>vrlld vd rs1 rs2</code>	
	strided store	<code>vsst vs rs1 rs2</code>	
	random store	<code>vrst vs rs1 rs2</code>	
Arithmetic	set duplicate	<code>vsetup vd rs</code>	n
	shift immediate**	<code>vshi vd vs rs</code>	n
	rotate immediate**	<code>vroti vd vs rs</code>	n
	shift register**	<code>vshr vd vs1 vs2</code>	$n \log(n)$
	addition	<code>vadd vd vs1 vs2</code>	n
	subtraction	<code>vsub vd vs1 vs2</code>	$2n$
	multiplication	<code>vmul vd vs1 vs2</code>	$n^2 + 5n$
	min/max	<code>vmin/max vd vs1 vs2</code>	$2n$
	xor	<code>vxor vd vs1 vs2</code>	n
comparison	<code>vgte(lt)(e)(n)eq vs1 vs2</code>	n	

*Compute latency of bit-serial signed integer operations based on precision (n).

**Shift and rotate operations include *right* (r) or *left* (l) variants.

To use MVE data types and instructions in the C/C++ program, we developed a library of supported variables and intrinsics. MVE variables are declared as `__mdv` as an acronym for Multi-Dimensional Variable, concatenated by the data type suffixes. Programmers include this library in the code and develop their kernels using MVE with a comparable level of effort to that required for other long-vector architectures (e.g., RVV [5] and SVE [80]). We developed an in-house compiler infrastructure and applied the following compiler optimizations on the data-parallel MVE kernels. Executable binaries are decoded in the front-end modules of the core, the scalar back-end pipelines execute scalar instructions, and long-vector in-cache instructions are issued to the MVE Controller.

G. Compiler

Compiler support of MVE is similar to long-vector architectures with the following considerations:

Register Count. While conventional architectures define a constant number of PRs, MVE PRs are limited by the number of word-lines (256) and the width of live PRs (Figure 2(b)). To simplify register allocation, we employ a single data width for a kernel. Using Liveness Analysis [32], compiler detects the widest PR width of a kernel and injects a config instruction (Table II) to set the PR width as a control register. MVE controller maps the PRs to the word-lines using this CR.

Register Allocation and Instruction Scheduling are two Code Generation optimizations that improve register spills and ILP. We focus on vector register pressure as it is critical to MVE due to the limited number of PRs and the high spill cost of wide in-cache vector registers. We use *list-hybrid* instruction scheduler [60], a bottom-up List Scheduling algorithm that tries to keep the live registers less than the target machine’s PR count and shorten register live ranges by scheduling instructions that do not generate register spills close to their use. Moreover, we employ *Greedy Register Allocation* [67], which minimizes register spills by extensively splitting live ranges, reducing register interference.

IV. COMMON DATA-PARALLEL PATTERNS

To illustrate the expressibility of the MVE ISA, we show the implementation of common data-parallel patterns of the evaluated mobile kernels. The instructions are listed in Table II concatenated with the data type suffixes.

Matrix transposition is employed in the Machine Learning (*XNNPACK* [40]), image/video codecs (*Kvazaar* [86] and *libjpeg* [57]), and cryptography (*boringsssl* [38]) libraries. The following code snippet shows the transposition of an $M \times N$ matrix using MVE. For simplicity, in this example, we assume both dimensions are smaller than the number of SIMD lanes. Any kernel starts with configuring the dimension count, lengths (Line 3), and stride CRs (L5). The main loop of the transpose kernel loads the input matrix columns vertically using the stride values of N and 1 (L9) and stores the output matrix rows horizontally with the stride values of 1 and N (L12). To transpose a 512×49 matrix (one of MobileNet-V1 [43] kernels), the MVE implementation requires only 4

iterations, while the 1D implementation needs 49 iterations to load/store input columns separately.

```

1 void transpose(int input[M][N], int output[N][M]){
2 // 2D: M output columns (DIM0), 8192/M rows (DIM1)
3 vsetdimc(2); vsetdiml(0, M); vsetdiml(0, 8192/M);
4 // load stride(DIM0) = N, store stride(DIM1) = N
5 vsetldstr(0, N); vsetststr(1, N);
6 for (int i = 0; i < N; i += 8192/M) {
7 // LD 8192/M columns: stride(DIM0) = MODE3 (N)
8 //                               stride(DIM1) = MODE1 (1)
9 __mdvdw in_val = vlds_dw(&input[i], 3, 1);
10 // ST 8192/M rows: stride(DIM0) = MODE1 (1)
11 //                               stride(DIM1) = MODE3 (N)
12 vsts_dw(&output[i*M], in_val, 1, 3);
13 }
14 }

```

Reduction is employed in the Network (*Checksum* [12]), audio/image processing (*libwebp* [59] and *webaudio* [37]), and compression (*zlib* [7]) libraries. The reduction of an input array to 8K elements (number of SIMD lanes) is simply implemented using 1D vector loads and additions. The reduction beyond 8K elements repeatedly splits the vector register into two halves and then reduces to half of the elements. Instead of supporting arbitrary data movements between SRAM arrays and bit-lines to align the half registers, we mask off the first half of the register using dimension-level mask operations (L6) and store the second half of the vector register to the memory using 2D vector stores (L8). Next, we set the vector length to half (L10), load the second half into a temporary register (L11), and reduce the half vector registers (L13). We repeat this vertical reduction step until we reduce the array to 256 elements (5 steps) after which the reduction proceeds in the CPU core, as in-cache computing is not beneficial after this point due to the significant arithmetic operation latency.

```

1 __mdvdw vertical_reduction_step(__mdvdw a, int M) {
2 int tmp_mem[M];
3 // Split M SIMD lanes into 2 M/2-element halves
4 vsetdimc(2); vsetdiml(1, 2); vsetdiml(0, M/2);
5 // Mask off the first half (element 0)
6 vunsetmask(0);
7 // Store the second half to the temp memory
8 vsts_dw(tmp_mem, a, 1);
9 // Load the second half into a register
10 vsetdimc(1); vsetdiml(0, M/2);
11 __mdvdw tmp_val = vsl_d_dw(&tmp_mem[M/2], 1);
12 // Reduce the two M/2-element registers
13 return vadd_dw(a, tmp_val);
14 }

```

Irregular accesses require random vector loads and stores. We observe this pattern in two scenarios: (a) Sparse computation: for example, in the *SPMM* kernel of the *XNNPACK* [40] library, the input matrix is sparse and compressed in a CSR format. Core computes the non-zero input cell addresses based on the row-pointers, and MVE randomly loads and replicates them horizontally. Similarly, core computes the weight row addresses corresponding to non-zero input cells, and MVE randomly loads them sequentially. (b) Data pointers: the image processing (*libjpeg* [57], *libpng* [58], and *libwebp* [59]) and graphics (*Skia* [39]) libraries maintain the frame rows in random memory locations. To operate on multiple rows

simultaneously, we need to load or store different rows from random base addresses. The following code snippet shows only the memory access pattern of the *libjpeg*'s *upsample* kernel. The input pixels are loaded from random input row pointers and each pixel is replicated twice (L10). The output results are stored to output pointers sequentially (L14).

```

1 void upsample(char* input[M], char* output[2M]) {
2   // 3D: replicate 2 pixels (DIM0)
3   vsetdimc(3); vsetdiml(0, 2);
4   // M columns (DIM1), 8192/(2M) rows (DIM2)
5   vsetdiml(1, M); vsetdiml(2, 8192/(2M));
6   for (int n = 0; n < N; n += 8192/(2M)) {
7     // Random LD rows from input pointers
8     // Load pixels in a row: stride(DIM1)= MODE1(1)
9     // Rep. pixels twice: stride(DIM0)= MODE0(0)
10    __mdvb rows_val = vrd_b(&input[n], 0, 1);
11    // Random ST rows to output pointers
12    // Store sequentially: stride(DIM0) = MODE1(1)
13    //                               stride(DIM1) = MODE2(2)
14    vrst_f(&output[n], rows_val, 1, 2);
15  }
16 }

```

Multidimensional replication is prevalent in all data-parallel kernels. For example, the row-wise *GEMM* kernel of the *XNNPACK* [40] library loads and replicates the input (L12) and weight (L15) elements horizontally (DIM0) and vertically (DIM1), respectively. Setting the i^{th} stride to zero replicates across the i^{th} dimension as shown in the following code.

```

1 void GEMM_Replication(float input[N][K],
2   float weight[K][M], float output[N, M]) {
3   // 2D: M output columns(DIM0), 8192/M rows(DIM1)
4   vsetdimc(2); vsetdiml(0, M); vsetdiml(1, 8192/M);
5   // load stride(DIM1)= K, store stride(DIM1)= M
6   vsetldstr(1, K); vsetststr(1, M);
7   for (int n = 0; n < N; n += 8192/M) {
8     __mdvf acc_val = vsetdup_f(0);
9     for (int k = 0; k < K; k++) {
10      // LD an input column: stride(DIM1)= MODE3(K)
11      // Rep. horizontally: stride(DIM0)= MODE0(0)
12      __mdvf input_val = vsld_f(&input[n*K+k], 0, 3);
13      // LD a weight row: stride(DIM0)= MODE1(1)
14      // Rep. vertically: stride(DIM1)= MODE0(0)
15      __mdvf weight_val = vsld_f(&weight[k*M], 1, 0);
16      acc_v = vadd_f(acc_v, vmul_f(input_v, weight_v));
17    }
18    // ST sequentially
19    vsst_f(&output[n*M], acc_val, 1, 3);
20  }
21 }

```

V. DESIGN

A. Core Micro-architecture

MVE instructions are fetched, decoded, and pushed to both the Reorder-Buffer (ROB) and Load Store Queue (LSQ). We do not support the out of order and speculative issue of MVE instructions. Hence, the LSQ prevents the reordering of scalar loads and MVE stores. Once committed, MVE instructions are issued to the L2 cache at the head of the ROB, and retired from the LSQ and ROB. Because none of the MVE instructions write to the scalar registers (Table II), no write back is required for these instructions.

MVE stores, however, are pushed to the write buffer until completed and acknowledged by the MVE controller. The in-cache MVE store execution takes many cycles, which stalls the younger scalar loads in the ROB. To minimize unnecessary stalls, we provision an Address Decoder in the LSQ. The address decoder maintains *DimCount*, $Dim_{[0:3]}.Length$, and $Dim_{[0:3]}.Stride$ CRs that are updated upon the issue of the config instructions to the cache. When a MVE store is committed and pushed to the write buffer, the address decoder computes an *address range* following Equation 2. Using this address range, the write buffer looks up for memory dependency between the scalar loads in the ROB and MVE stores in the write buffer.

$$Range = Base + \sum_{i=0}^3 Dim_i.Length \times Dim_i.Stride \quad (2)$$

B. Cache Architecture.

Figure 6 shows the new modifications to the cache to enable the execution of MVE in the pink color:

MVE controller receives MVE instructions from the core in the program order and enqueues them to the *Instruction-Q*. When decoding a config instruction, MVE controller sets the CR values similar to the Address Decoder in the core. The logical registers are flattened out to the physical registers based on the dimension lengths, mapped to the *Data Arrays*, and issued to the *Finite State Machines* (FSM). FSMs further decode the instructions to micro-operations (μops) that control the *Row Decoders* and *Logic Peripherals* of SRAM arrays.

Control blocks. Augmenting each SRAM array with an independent FSM results in high area overhead. Therefore, we use a coarser granularity of four SRAM arrays for a *Control Block* (CB) and use a single FSM for each CB [35]. Due to the *dimension-level mask operations*, some CBs can be masked off of a MVE instruction. Therefore, MVE controller orchestrates the non-blocking execution of CBs by keeping a *mask bit-vector* that shows to which CBs each instruction must be issued. If a CB is not masked off, MVE controller issues the instruction to that CB.

MVE controller keeps a PC for each CB, which points to the instructions in the *Instruction-Q*. When a CB completes an instruction, it interrupts the MVE controller by raising the *ACK* signal. MVE controller unsets the corresponding bit-vector of the completed instruction. While increasing PC, MVE controller jumps over the instructions whose bit-vector is masked off for that CB. When the mask bit-vector of an instruction is all unset, it is dequeued from the *Intrinsic-Q*. The MVE ISA does not support any register-to-register permutation or shuffling, and any data transfer between SRAM arrays and bit-lines is through the memory (Table II). For that, we make sure there is only one load or store instruction executed in parallel in all CBs. Thus, MVE controller blocks on vector memory accesses until all CBs finish executing it.

Strided and random memory access execution. While issuing a memory access to a CB, MVE controller calculates the individual addresses using base address(es), stride

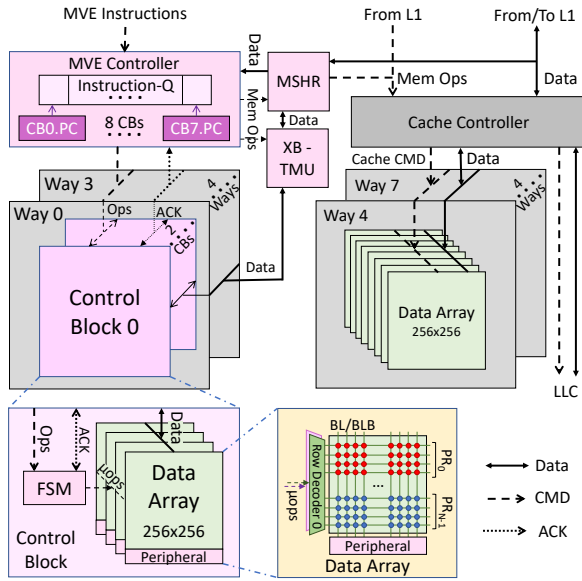


Fig. 6. MVE adds pink modules to the Cache Architecture.

modes, and CRs (Algorithm 1 and Equation 1). While there are opportunities to coalesce the memory accesses in the MVE controller based on the stride semantics, we decided to simplify the controller and use Miss Status Holding Registers (MSHR) for this purpose. The calculated addresses of each SIMD lane is sent to the MSHR, loaded from the regular half of the L2 cache, and delivered to the *Transpose Memory Unit (TMU)*. TMU is composed of 8T transpose bit-cells that can access data in both vertical and horizontal directions [31]. TMU is sized to maintain a physical register for a CB (1024 elements). The data words are routed to their correct vertical locations in the TMU SRAM cells using a *crossbars (XB)*. When all elements of a CB are received, the MVE controller signals the corresponding CB to read the register bit slices from the TMU horizontally and write to the data arrays. The store instructions require the opposite of the above process.

C. Discussion

Cache Coherency. Conventional cache coherency directories keep a single cache line state for the L1 and L2 caches of each core. However, in MVE, the L2 cache accesses memory for in-cache loads and stores independently of the core and the L1 cache. Consequently, cache levels are no longer coherent. We observe that the baseline L2 cache is strictly inclusive and the tag array contains a *presence* bit for each cache line, indicating if it is valid in the L1 cache [11]. To maintain the coherency with the L1 cache, we enable the MVE controller to check the *presence* bit of the tag array. Upon a cache hit for the in-cache memory access, the MVE controller checks the *presence* bit and evicts the cache line from the L1 cache if it is set. An inclusive L2 cache miss guarantees that the data is not in the L1, ensuring coherency between the L1 and L2.

What if in-cache computing is not needed? We carefully equip half of the cache ways [35] with in-cache computing while preserving their storage capabilities for scalar or SIMD applications. MVE does not permanently disable half of the cache banks to support the compute mode. Cache banks oper-

ate as regular cache when not used for in-SRAM computing. For workloads that do not benefit from long-vector execution, we default to normal CPU execution with regular cache usage. To switch from the normal cache to in-cache computing for long-vector applications, MVE flushes dirty cache lines. Based on a prior heuristic of 50% L2 cache lines being dirty [50], this process takes less than 2% of the execution time of the evaluated benchmarks. On the other hand, switching compute-cache to normal-cache only requires modifying a CR with negligible slowdown to the workload.

VI. EVALUATION METHODOLOGY

Benchmarks. We evaluate MVE using 44 data parallel kernels of 12 real-world mobile libraries from the Swan benchmark suite [49] as listed in Table III. For a detailed analysis and comparison with prior work, we select 11 kernels with various dimensions and data-parallel patterns (Section IV).

TABLE III
EVALUATED LIBRARIES

Domain	Library	#Kernels	Dataset	Dim
Linear Algebra	Linpack [30]	1	512K	1D
Machine Learning	XNNPACK [40]	2	156 CNN Layers	2D
Signal Processing	CMSIS-DSP [14]	3	192K	1D
Video Processing	Kvazaar [83]	4	1280×720	3D
Image Processing	libjpeg [57]	5	1280×720	2-4D
	libpng [58]	3		
	libwebp [59]	7		
Graphics	Skia [39]	4	1280×720	1-3D
Audio Processing	Webaudio [37]	5	32S×44.1kHz	1-3D
Data Compression	zlib [7]	2	128KB	1-2D
Cryptography	boringsssl [38]	3	128KB	1-2D
String/Network Utilities	Arm Optimized Routines [12]	5	128KB	1-2D

Mobile platform. Table IV shows the baselines using Qualcomm Snapdragon 855 SoC: packed-SIMD (Arm Neon) execution of Arm Cortex-A76 core [11] and Qualcomm Adreno 640 GPU. We use four L2 cache ways for data storage and four cache ways (32 SRAM arrays) for in-cache computing.

TABLE IV
QUALCOMM SNAPDRAGON 855 BASELINES

Configuration	Detail
Scalar core	2.8GHz, 4-way out-of-order, 128 entry ROB
Vector engine	2 128-bit Advance SIMD units + crypto and FP16 ext
L1-I cache	64KB, 4-way, 4 cycle latency, 20 MSHRs
L1-D cache	64KB, 4-way, 4 cycle latency, 20 MSHRs
L2 cache	512KB, 8-way, Private, Inclusive, 12 cycle latency, 46 MSHRs
LLC	2MB, 8-way, Shared, Inclusive, 31 cycle latency, 64 MSHRs/way
MVE	32 8-KB SRAM Arrays, 4-SA CB, 2KB Intrinsic-Q
GPU	2 cores, 384 ALUs, 685MHz, 1MB on-chip memory

Performance modeling. We developed a synthetic MVE intrinsic library that emulates 29 intrinsics for 6 data types and validated the functional correctness by comparing the outputs with the Arm Neon kernels. To generate instruction traces, we implemented a DynamoRIO client [42] that dumps the dynamic instructions on an Armv8.2-A server CPU (same as the mobile processor) while replacing function calls to the intrinsic library with their corresponding opcodes. Our

compilation infrastructure performs register allocation and instruction scheduling to the in-cache registers and MVE instructions. We then built a trace-driven, cycle-accurate simulator, faithfully modelling the micro-architecture of an Arm processor with the configurations of Table IV and cache architecture components explained in Section V and Figure 6. We use the bit-serial in-SRAM instruction latency of Duality Cache [35]. Our simulator injects memory accesses to the Ramulator [51] to model the memory latency and bandwidth.

Power and area modeling. We use the bit-serial in-SRAM computing energy parameters from [31] and evaluate cache access energy using CACTI [64]. *Dynamic* CPU and GPU energy consumption are measured using *Batterystats* [28] and *Trepan profiler* [70]. We take the TMU, XB, FSM, and Peripheral area from prior work [31], [35] and scale the numbers to MVE architecture requirements. We implemented the controller and address decoder in RTL and synthesized it with a 15nm CMOS library. MSHR area is evaluated using CACTI [64]. Scalar CPU core and GPU area are estimated using die shots [3], [41], and Arm Neon area is generously evaluated using a vector engine design [21]. We carefully scale all area and energy numbers to 7nm using equations of [81].

Prior work. For Duality Cache [35], we implement kernels in CUDA and run them on GPU Ocelot emulator [29] to capture dynamic PTX trace. We calculate compute cycles using our in-cache operation latencies and simulate memory accesses by Ramulator [51]. For BH, BP, and AC schemes, we implement kernels with various algorithms optimized for their number of SIMD lanes and in-cache registers. We ignore different operational frequencies and architectural contributions of prior work to demonstrate the benefits of MVE for various in-SRAM computing schemes in a similar hardware configuration. The compiler and trace-driven simulator are configured with in-cache register count, number of SIMD lanes per SRAM array, and compute and data movement latencies based on prior works [9], [10], [19]. To compare MVE with RISC-V RVV [5], we implement workloads using optimized algorithms for only 1D vector instructions.

VII. RESULTS

A. Performance and Energy Analysis

MVE vs. Arm Neon. Figure 7(a) shows the execution time of MVE normalized to Arm Neon. Due to the limited space, we only show the average for all kernels of a library. MVE outperforms Neon by $2.9\times$ across all evaluated mobile kernels, showing that MVE efficiently exploits the higher compute throughput of in-cache computing. The execution time is classified as 40.4% idle, 24.7% compute, and 34.8% data access time, on average. MVE performance improvement increases in kernels with lower precision (see Section VII-E). So, MVE significantly outperforms Neon for *libpng*, *libjpeg*, *libwebp* (image codecs), *Skia* (graphics), and *Arm optimized routines* (string/network utility) libraries, which operate on 8-bit pixel values and characters.

The idle time is when the control blocks (CBs) have no MVE instructions to execute. It increases when the portion of

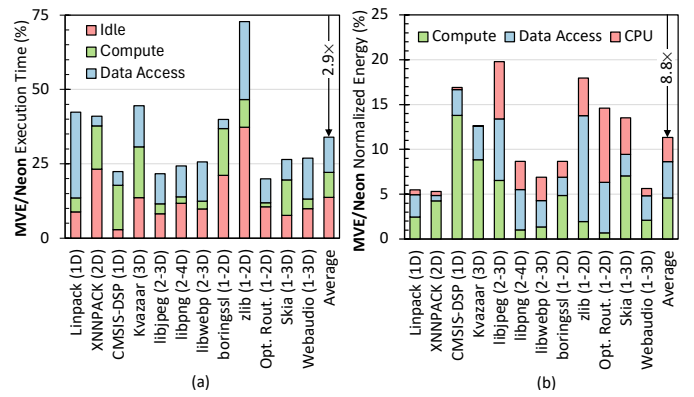


Fig. 7. (a) Execution time and (b) energy consumption of MVE normalized to packed-SIMD Neon model.

scalar instructions is higher. For example, the *Adler32* kernel of the *zlib* library (compression) requires the reduction kernel (explained in Section IV). In the vertical reduction based on the tree algorithm, many CBs are idle. The scalar core reduces the elements from 256 to 1, while the CBs are idle. The idle time drops the *zlib* performance improvement to only 37%.

MVE improves the energy consumption by $8.8\times$ on average as shown in Figure 7(b). Significant energy reduction in MVE is because of two reasons: (a) the long-vector execution model effectively packs numerous operations into one multi-dimensional instruction, reducing CPU instructions and energy. (b) the in-SRAM computing operations are energy-efficient [8]. In addition, in-cache computing prevents the data transfer from the L2 cache to the core’s register files and back.

MVE vs. GPU and DSP. Mobile Application Processors integrate specialized accelerators like GPU, DSP (NPU), ISP, and SPU to accelerate *specific application domains* such as multimedia processing, machine learning, image signal processing, and security. In contrast, MVE is a *general-purpose* approach to flexibly accelerate all application domains.

Figure 8 compares the execution time and energy consumption of MVE with Adreno 640 GPU. Despite $13.6\times$ lower 32-bit integer MAC throughput, MVE outperforms GPU by $9.3\times$ and reduces energy by $5.2\times$ because of two primary reasons:

(a) *Data transfer* incurs a significant overhead for GPUs. To reduce this cost, we utilize unified physical memory following the Snapdragon OpenCL Optimization Guide [71]. While we do not account for the cost of memory allocation, transferring data from complex C++ objects to pinned C array pointers in the unified memory region incurs a substantial overhead, taking $6.9\times$ longer than the average execution time of MVE.

(b) After discounting the data transfer time, MVE still provides an average speedup of $2.4\times$. This is attributed to the high *kernel launch overhead* of OpenCL Runtime library [49] and core-GPU communication via the system fabric. Similarly, DSP experiences kernel launch overhead, including latencies introduced by *ADSPRPC*, *skel*, and *kernel object* transfers, *stub/skel* parameter de/serialization, and *FastRPC* remote calls through the system fabric [17], [69]. Conversely, MVE avoids these overheads by leveraging the fine-grained scalar-vector instruction interleaving of the SIMD execution model.



Fig. 8. Performance (primary Y-axis) and Energy (secondary Y-axis) consumption of Adreno 640 GPU normalized to MVE.

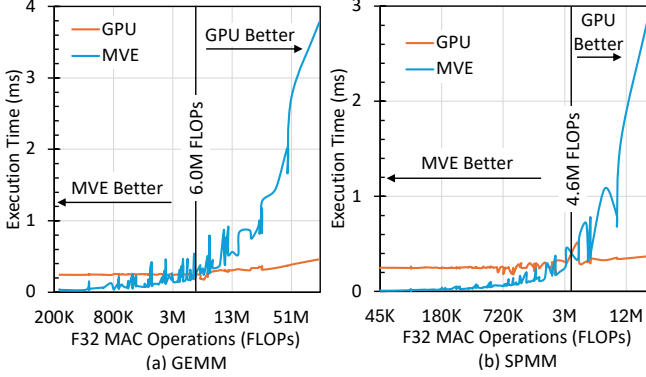


Fig. 9. GEMM and SpMM execution time of MVE and Adreno 640 GPU for different operation counts (matrix sizes).

Finally, note that we compare a single-core MVE performance with the GPU. Augmenting all 8 cores of Snapdragon 855 SoC with in-cache computing would further increase the performance superiority of MVE compared to a single GPU.

To compare MVE and GPU in more depth, we take the OpenCL *GEMM* and *SpMM* implementations from CLBlast [65] and cISPARSE [24] libraries, and evaluate them for different matrix sizes employed in 152 layers of 13 mobile Convolutional Neural Networks [40] using Figure 9. MVE outperforms GPU up to matrix multiplications with 6.0M and 4.6M FLOPs. In large problem sizes, the higher throughput of GPU offsets its kernel launch overhead. On the other hand, MVE requires only 8K DLP to fully utilize the SIMD lanes, so it is preferred for smaller problem sizes.

B. Multi-dimensional ISA Benefits

Figure 10 and Figure 11 compare the performance and dynamic instruction count of MVE with a 1D long-vector ISA extension such as RISC-V RVV [5] while using the same underlying bit-serial in-cache computing engine. We select various kernels for this comparison with different dimensions from 1D to 3D. MVE significantly reduces the idle time of the kernels that require multi-dimensional accesses, and improves the performance by 2.0 \times on average across all selected kernels. To mimic a multi-dimensional access using RVV, we use predicate operations to mask 1D strided memory accesses and (un)pack each 1D segment of data structure separately in a piece of vector registers. This approach generates $\frac{\#SIMD\ Lanes}{length(1D\ segment)}$ config (mask), partial 1D memory accesses,

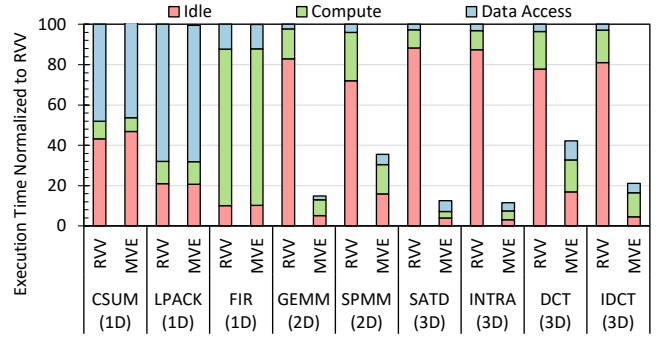


Fig. 10. MVE Performance compared to RISC-V RVV [5] when targeting the same underlying bit-serial in-cache computing engine with 8K SIMD lanes.

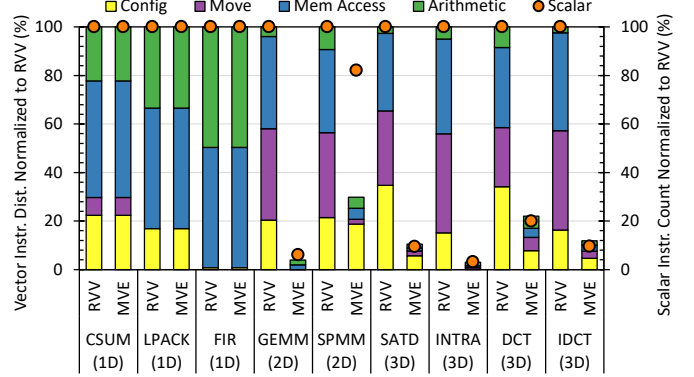


Fig. 11. MVE and RISC-V RVV [5] dynamic vector instruction distribution (left Y-axis) and dynamic scalar instruction count (right Y-axis).

and move instructions for each multi-dimensional memory access. Figure 11 (left Y-axis) illustrates that MVE reduces the number of dynamic vector instructions by 2.3 \times , on average.

Across various GEMM kernels in the XNNPACK library [40], RVV significantly increases dynamic vector instructions in smaller output matrices (less 1D parallelism) compared to MVE. For instance, a 128×3136 output matrix from MobileNet V1 [43] requires approximately $\frac{8192}{3136} \approx 3$ mask, partial memory accesses, and move instructions across three 1D segments (output rows) to occupy 8K SIMD lanes. This results in a 5.3 \times increase in the vector instruction count compared to MVE. Another 122×784 output matrix from ShuffleNet V2 [61] involves $\frac{8192}{784} \approx 11$ 1D segments, leading to a 13.0 \times increase in the vector instructions.

Additionally, more partial memory accesses require more scalar address calculation instructions. Hence, Figure 11 (right Y-axis) shows that MVE reduces the number of dynamic scalar instructions by an average of 2.0 \times compared to RVV.

C. Comparing In-SRAM Technologies

VRAM [9], EVE [10], and CAPE [19] employ the RVV ISA extension to instruct a bit-parallel (BP), bit-hybrid (BH), and Associative Computing (AC) in-SRAM engine. Figure 13 shows that MVE improves the performance of all in-SRAM computing schemes when compared with RVV. Numerous partial memory accesses of RVV drop CB utilization of the BS to 23%, BH to 25%, and BP to 24%. MVE efficiently encode multi-dimensional memory accesses in only one vector instruction, increasing the CB utilization of BS to 60%, BH

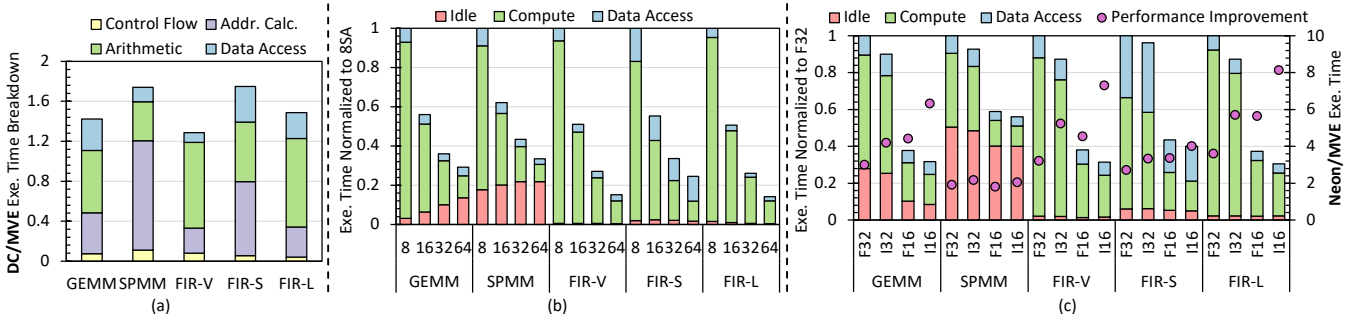


Fig. 12. (a) Performance comparison with Duality Cache [35]. (b) Performance scalability using various numbers of SRAM Arrays (SA), and (c) Performance sensitivity to the data precision.

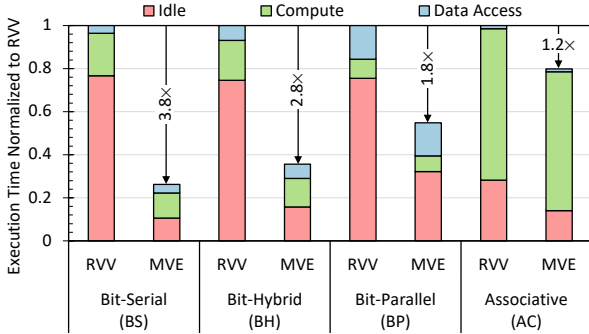


Fig. 13. Performance improvement of MVE compared to RISC-V RVV [5] for different in-SRAM computing schemes employed in VRAM [9], EVE [10], and CAPE [19].

to 55%, and BP to 41%. Among these schemes, BP still shows relatively lower CB utilization. This is because BP enjoys less compute latency at the cost of fewer SIMD lanes. Therefore, the in-cache engine is faster in consuming the long-vector instruction, which increases the pressure on the core to issue instructions at a higher rate. Less idle time improves the performance of BS, BH, and BP by 3.8 \times , 2.8 \times and 1.8 \times . While MVE also cuts down the idle time of AC by 2.0 \times , this in-SRAM computing scheme does not benefit significantly from a multi-dimensional ISA. This is because the latency of the AC arithmetic operations is 4–8 \times higher than BS, hence, 70% of AC execution time is spent on arithmetic operations.

Duality Cache [35]. Figure 12 (a) demonstrates that MVE, using a SIMD model, achieves an average performance improvement of 1.5 \times over the prior SIMT-based in-cache computing design, Duality Cache [35]. The performance improvement is primarily due to two reasons: *First*, MVE reduces compute cycles as it requires fewer in-SRAM computing operations. In the SIMT model, all operations (control flow, address calculation, and arithmetic) are offloaded to the in-SRAM computing engine and performed individually by all SIMT lanes. In contrast, MVE executes control flow and base address calculations once on the scalar core, while the cache controller computes memory addresses for each SIMD lane using the stride semantics of MVE memory accesses. Therefore, the SIMT model removes the idle cycles of the in-SRAM computing engine at the cost of more in-SRAM operations. So, the SIMT model is ideal for large server-class in-SRAM engines, where control-flow divergence poses

a challenge, while the SIMD model is better suited for small mobile caches that prioritize low latency. *Second*, data access time of the SIMT model takes 1.6 \times longer than MVE. This is because the SIMT model keeps all scalar and vector variables in the scarce in-cache physical registers, leading to frequent register spills and fills. These operations are particularly costly due to the large number of data elements in the in-cache physical registers (8K elements).

D. Scalability Analysis

Figure 12 (b) shows the performance scalability of MVE with different SRAM array counts. These baselines are designed by keeping the 512 KB L2 cache intact and augmenting the core with an additional 8 to 64 SRAM arrays dedicated for MVE. This result shows that increasing SRAM arrays by 8 \times increases MVE performance from 3.0 \times (SpMM) to 6.7 \times (FIR-L). Idle time is the primary bottleneck for scaling the performance of MVE for the massive server-class caches.

E. Sensitivity to Bit Precision

Figure 12 (c) shows the impact of bit precision on the execution time of MVE (left Y-axis) and its performance improvement over Neon (right Y-axis) with two takeaways: *First*, MVE shows greater performance improvement over Neon at lower precisions, indicating that in-SRAM computing benefits more from lower bit precisions than CMOS-based processors. This is because in-SRAM computing relies on a bit-serial paradigm with an arithmetic complexity of $\mathcal{O}(\text{precision}^2)$. So, bit precision has a quadratic effect on the throughput. In contrast, Neon ASIMD units achieve linear scaling with lower bit precision, as they can pack more data elements into a SIMD register. *Second*, idle cycles in MVE do not decrease significantly with lower precision. This is because CBs execute lower-precision in-SRAM instructions much faster, outpacing the rate of issuing instructions by the core.

F. Area Analysis

Table V evaluates the area overhead of MVE compared to Snapdragon 855 mobile SoC. While augmenting a scalar data path with the Neon register files and ALUs incur 16.3% area overhead, MVE transforms the cache structures to a long-vector engine with a negligible 3.6% area overhead to the scalar core. This area overhead is similar to the findings of the prior work, e.g., 3.5% [35] and 2% [31]. MVE area is

dominated by FSM controllers, which decode MVE instructions to the μ ops. This table further shows the significantly larger area of GPU. Hence, a general-purpose MVE design offers both performance and energy benefits over dedicated hardware components at a negligible silicon area, making it an attractive solution for the cost-sensitive mobile industry.

TABLE V
OVERHEAD TO THE SCALAR CORE AREA (1.07mm² [3])

Module	Source	Area (mm ²)	Overhead (%)
Arm Neon	[21]	0.1741	16.321
MVE	Controller	RTL	0.0043
	MSHR	CACTI	0.0018
	TMU	[31]	0.0053
	XB	[35]	0.0039
	FSM	[35]	0.0123
	Peripheral	[35]	0.0063
	Address Decoder	RTL	0.0042
	Total	–	0.0382
Adreno 640 GPU	[41]	11.1908	–

VIII. RELATED WORK

Domain-specific in-cache computing. In-cache computing is specifically studied for different domains such as Machine Learning [8], [31], [87], Automata Processing [72], [73], [82], Image Processing [16], and Data Encryption [89]. However, domain-specific acceleration requires extra effort for customizing data layout of the cache and dataflow between core and in-cache elements. A general-purpose execution model such as MVE lifts this burden from the programmers, unleashing the power of in-cache computing for other domains.

General-purpose ISA design for in-cache computing. Several works have extended the scope of in-cache computing for general applications. We already comprehensively discuss Duality Cache [35], CAPE [19] and EVE [10]. Kooli *et al.* [54], [55] propose a general-purpose SIMD model for in-cache computing, integrating the execution flow with the CPU. They also introduce an in-place shuffle operation to accelerate cryptography, image processing, *etc.* Blade [79] proposes circuit-level solutions for in-cache computing to operate at high-frequency and low-voltage of mobile processors. The architectural contributions of these prior works are orthogonal to this paper. MVE could be employed to enhance the performance of all prior In-SRAM architectures (Section VII-B).

Prior work demonstrates the multi-dimensional access pattern of in-memory databases where the data can be accessed column and row-wise in a logical linear address space. GS-DRAM [76] proposes changes in the DRAM controller to fetch power-of-two strided access patterns independently from multiple DRAM chips, improving DRAM bandwidth utilization. MDACache [36], RC-NVM [56], and MVC [33] modify the computing stack and cache architecture to enable vertical and horizontal access to the non-volatile memories, improving cache line utilization. These proposals can complement MVE and be employed to enhance the DRAM memory bandwidth.

Mobile vector processing. Big.VLITTLE [84] re-purposes little cores in the big.LITTLE architecture of mobile processors as a decoupled vector processing engine without adding area-expensive components such as vector register files

and wide execution pipelines. MVE supports a larger SIMD capacity tightly integrated into the scalar core by repurposing half of the processor’s L2 cache. PUMICE [88] proposes out-of-order dispatch of in-cache long-vector instructions to hide the command distribution overhead of CAPE [19]. MVE architecture can also employ this technique to reduce idle time.

Long-vector and Matrix processing. The emergence of multimedia extensions two decades ago inspired designs to enhance the DLP exposed to SIMD engines. MOM [25], [26] proposed 2D SIMD instructions while supporting flexible vector length and stride in the second dimension. Breeze [85] and CSI [23] proposed CISC-based instructions to encode all operations, data access patterns, and nested loop semantics for offloading to a streaming media processor. Motorola 56000 [52] and Texas Instruments TMS320C5x [44] DSPs employ sophisticated DO loop and strided address calculation instructions to reduce the control flow and address calculation overhead. More recently, Nvidia server GPUs have incorporated Tensor Memory Accelerator (TMA) units [66] capable of bulk copying 1-5D tensors from global memory to on-chip shared memory. Further, ISA extensions are proposed for machine learning workloads in server processors. Intel Advanced Matrix Extension (AMX) [45] and Arm Scalable Matrix Extension (SME) [13] are 2D matrix ISA extensions, enabling high-performance 1K-bit and 2K-bit matrix operations. AMX has two main components: specialized loads to fixed-size tiles composed of eight 2D registers, each 1KB in size, and Tile Matrix Multiplication Units, which perform matrix-multiply computations.

As opposed to these designs, MVE is a *long-vector ISA* extension specifically targeting tightly coupled in-cache computing engines for mobile cores and capturing the semantics of data-parallel computation across multiple dimensions systematically. Besides, MVE encodes irregular computations using random memory accesses and efficient dimension-level masked execution tailored towards mobile workloads.

IX. CONCLUSION

This work introduces a long-vector Multi-dimensional Vector ISA Extension (MVE) that abstracts away the in-cache computing as a tightly-integrated long-vector processing engine. MVE enables the high utilization of numerous SIMD lanes using multi-dimensional strided and random memory accesses, and efficient dimension-based masked execution. Using this ISA extension, MVE repurposes half of the L2 mobile caches for in-cache computing with a 3.6% area overhead. The long-vector in-cache architecture offers 2.9 \times performance improvement and 8.8 \times energy reduction, compared to a commercial mobile CPU vector baseline. Compared to the RISC-V RVV, MVE improves the in-cache engine utilization from 23% to 60% and improves the performance by 3.8 \times when targeting the same underlying bit-serial in-cache computing engine.

ACKNOWLEDGEMENTS

This work was supported in part by the NSF under the CAREER-1652294 and NSF-1908601 awards and by JST PRESTO Grant Number JPMJPR22P7.

A. Abstract

The artifact of this paper includes the in-cache computing simulator for MVE ISA, various implementations of the benchmarks, and instrumentation tools for baseline evaluation.

B. Artifact check-list (meta-information)

- **Program:** Scalar, Arm Neon, OpenCL, CUDA, MVE, and RVV implementations of evaluated Swan [49] benchmarks (Table VI).
- **Compilation:** Android NDK r23c for Arm Neon, Adreno OpenCL SDK v1.5 for mobile GPU, Clang 3.4+ for simulator, and CMake 3.7+ for DynamoRIO.
- **Software:** Git LFS.
- **Hardware:** Samsung Galaxy S10e for the packed-SIMD Neon and Adreno GPU baselines, an Armv8.2-A machine for generating the simulation traces, and any system for simulation.
- **Output:** CSV files generated by [automation scripts](#).
- **Experiments:** Arm Neon (mobile SIMD) and Adreno (mobile GPU) measurements on the mobile device, MVE and RVV simulations for bit-serial (BS), bit-hybrid (BH), bit-parallel (BP), and associative computing (AC) in-cache computing schemes.
- **Required disk space:** Approximately 65 GB
- **Preparation time:** Approximately 1 hour
- **Measurement/simulation time:** Approximately 24 hours
- **Publicly available:** Yes, available on [GitHub](#) and [Zenodo](#).
- **Code license:** Yes, [MIT License](#).
- **Workflow automation:** Yes, located in [benchmarks/scripts/](#).

C. Overview

This artifact consists of two parts for reproducing the results presented in the following figures: (i) Figure 7(a) (MVE vs. Arm Neon), (ii) Figures 8 and 9 (MVE vs. Adreno GPU), and (iii) Figures 10, 11, and 13 (MVE vs. RVV). The first part involves conducting measurements on a mobile device, while the second simulates the MVE and RVV kernels for the BS, BH, BP, and AC in-cache computing schemes. Both parts require access to specific hardware dependencies, particularly Arm-based machines. If you do not have access to these machines, we provide precomputed result files to bypass them.

Table VI shows all implementations [available here](#). We provide both Scalar and Neon implementations for all libraries; however, only the Neon implementations are used for comparison with the vector units (Arm Neon). The MVE implementation is also provided for all libraries. We selected 10 kernels with varying dimensions and implemented the following versions: (a) Using one-dimensional instructions only, for comparison with RVV, (b) Using OpenCL, to evaluate performance on the Adreno mobile GPU, and (c) Using CUDA, to study the performance of the Duality Cache (DC) [35]. Note that this artifact does not include the reproduction of Figure 12 (a) (MVE vs. DC), due to the complexities with DC’s simulation infrastructure (GPU Ocelot [29]).

How to access artifact? All the necessary codes, tools, and scripts are available in our [GitHub repository](#). This repository also includes large dynamic instruction and data flow graph files (approximately 2.5GB), which can be used to skip Steps 1 and 2 of Part 2 (Section E). If you wish to clone the repository while downloading these large files, install [Git](#)

TABLE VI
BENCHMARK IMPLEMENTATIONS.

Library	#Kernels	Scalar	Neon	MVE	RVV	OpenCL	CUDA
Linpack	1	✓	✓	✓	✓	✓	✓
XNNPACK	2	✓	✓	✓	✓	✓	✓
CMSIS-DSP	3	✓	✓	✓	✓	✓	✓
Kvazaar	4	✓	✓	✓	✓	✓	✓
Arm Opt. Routines	1 4	✓ ✓	✓ ✓	✓ ✓	✓ X	✓ X	✓ X
libjpeg	5	✓	✓	✓	X	X	X
libpng	3	✓	✓	✓	X	X	X
libwebp	7	✓	✓	✓	X	X	X
Skia	4	✓	✓	✓	X	X	X
Webaudio	5	✓	✓	✓	X	X	X
zlib	2	✓	✓	✓	X	X	X
boingssl	3	✓	✓	✓	X	X	X

LFS before cloning. Otherwise, set the environment variable `GIT_LFS_SKIP_SMUDGE=1` before cloning.

D. Part 1 – Mobile Measurements

Hardware dependencies. This step requires a Samsung Galaxy S10e device equipped with the Snapdragon 855 SoC. If you do not have access to this device, you can bypass this step by using the pre-generated CSV files located at `path/to/MVE/data/csv_files.tar.gz`.

Software dependencies. Mobile measurements require Android NDK r23c ([download from Android GitHub repository](#)) for cross-compilation, and Adreno OpenCL SDK v1.5 (available on [our GitHub repository](#)) and Adreno OpenCL shared library (available on [our GitHub repository](#)) for mobile GPU. In addition to these, we need [Android Debug Bridge \(adb\)](#) to enable shell access to the phone.

Installation. Install adb. Download Android NDK r23c, Adreno OpenCL SDK v1.5, and Adreno OpenCL shared library, and extract them. Run the following bash script to set up the cross-compilation infrastructure and compile the Arm Neon and Adreno GPU baselines.

```
export ANDROID_NDK_ROOT=path/to/android-ndk-r23c
cp -r path/to/MVE/tools/opencv-sdk-1.5/inc/CL
  $ANDROID_NDK_ROOT/toolchains/llvm/prebuilt/linux
  -x86_64/sysroot/usr/include/
cp path/to/MVE/tools/libopencv/libOpenCL.so
  $ANDROID_NDK_ROOT/toolchains/llvm/prebuilt/linux
  -x86_64/lib/
cd path/to/MVE/benchmarks
make phone_neon -j
make phone_adreno -j
```

Experiment Workflow. Connect the Samsung S10e device to your computer. Enable the [Developer Option and USB debugging](#). Run the following provided scripts to automatically generate `neon.csv` and `adreno.csv` results.

```
cd path/to/MVE/benchmarks
python scripts/profiler.py --core prime \
  --measurement performance --platform neon \
  --output neon.csv --verbose
python scripts/profiler.py --core prime \
  --measurement performance --platform adreno \
  --output adreno.csv --verbose
```

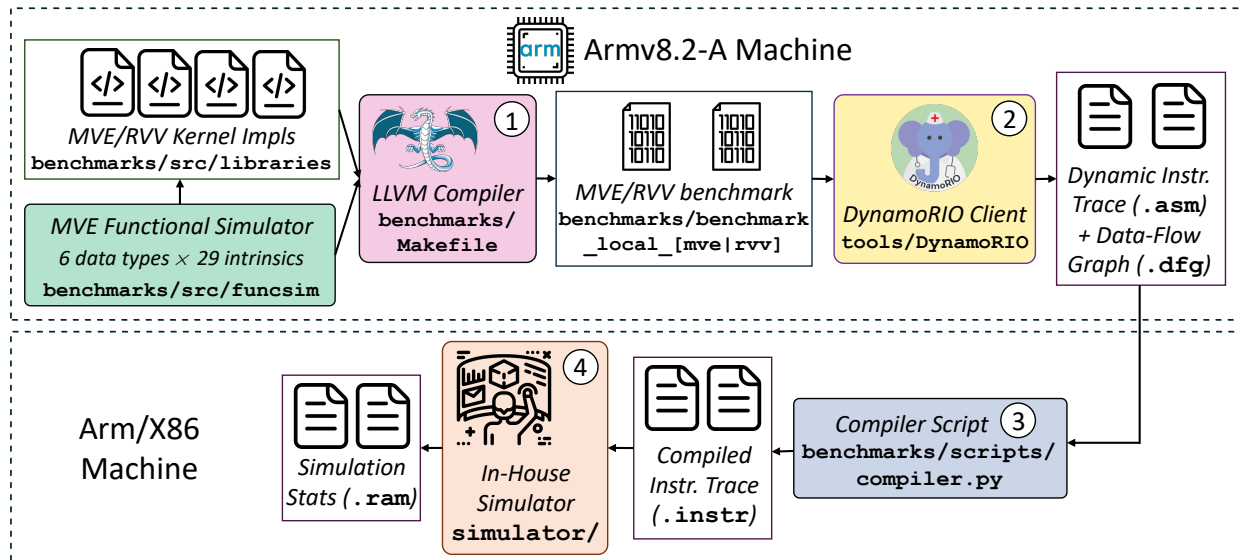


Fig. 14. Simulation takes four steps. Steps 1 and 2 must be executed on an Armv8.2-A machine. Steps 3 and 4 can be performed on any machine.

E. Part 2 – In-Cache Simulation

Overview. Figure 14 illustrates the four steps of the simulation process. Steps 1, 2, and 3 generate the instruction traces, while the final step 4 runs the simulations.

Hardware dependencies. Steps 1 and 2 require a machine equipped with the Armv8.2-A ISA. The remaining steps 3 and 4 can be executed on any machine. If you do not have access to this certain machine, you may skip the first two steps.

Software dependencies. We implemented a [DynamoRIO client](#) [42] to instrument the benchmarks and dump the dynamic instruction traces. We use [in-house simulator](#) for in-cache computing simulations.

Installation. Install the DynamoRIO client on a machine with Armv8.2-A ISA using the following script. If you do not have access to such a machine, you can skip this step.

```
cd path/to/MVE/tools/DynamoRIO/samples
mkdir build
cd build
cmake ..
make -j
```

To install our simulator, run the following script. Please note that building the simulator is mandatory, even if you plan to skip the first two steps of Part 2.

```
cd path/to/MVE/simulator
bash make_all.sh
```

Experiment Workflow. Simulation takes place in 4 steps using the following bash script. *Step 1* builds the MVE and RVV baselines. *Step 2* runs the MVE and RVV benchmarks and use the DynamoRIO client to generate a dynamic instruction trace (.asm) and a data-flow graph (.dfg) file for each kernel. *Step 3* compiles these files to the trace files for the simulator. *Step 4* runs the simulator and generates the simulation results (.ram). To configure the number of concurrent simulations, use the `-j [NUM_THREADS]` argument.

Finally, scripts are provided to parse the simulation results and generate the CSV files for any ISA (MVE and RVV) and in-cache computing scheme (BS, BH, BP, AC) combinations.

```
cd path/to/MVE/benchmarks
# Step 1: building the MVE and RVV kernels
make local_mve -j
make local_rvv -j
source ./set_env.sh
# Step 2: running DynamoRIO's instrumentation tool
python scripts/simulator.py --action benchmark \
  --directory ./data --verbose
# Step 3: compiling asm and dfg files into traces
python scripts/simulator.py --action compile \
  --directory ./data --verbose
# Step 4: running the simulations
python scripts/simulator.py --action simulate \
  --directory ./data -j [NUM_THREADS] --verbose
# Parsing the results
python scripts/simulator.py --action parse \
  --directory ./data --verbose
```

Skipping Steps 1 and 2. Skip the first two steps by using the generated (.asm) and (.dfg) files. First, ensure these files are downloaded (See Section C – How to access artifact?). Next, perform the following operations to extract these files and resume *Step 3*.

```
cd path/to/MVE/benchmarks
tar -xvzf ../data/data_bs.tar.gz
tar -xvzf ../data/data_bh.tar.gz
tar -xvzf ../data/data_bp.tar.gz
tar -xvzf ../data/data_ac.tar.gz
# Resume Step 3
```

F. Evaluation and expected results

The expected results are in the pre-generated CSV files located at `path/to/MVE/data/csv_files.tar.gz`. Use these files to fill out the first 10 sheets of the result Excel file, located at `path/to/MVE/data/Results.xlsx`. Completing these sheets will generate Figures 7(a), 8, 9, 10, 11, and 13.

REFERENCES

- [1] Android - secure and reliable mobile operating system. [Online]. Available: <https://www.android.com/>
- [2] Chromium. [Online]. Available: <https://www.chromium.org/Home/>
- [3] Kirin 990 5g dieshot. [Online]. Available: <https://xian333c.top/archives/526>
- [4] Pdfium. [Online]. Available: <https://pdfium.googlesource.com/pdfium/+master/README.md>
- [5] riscv-v-spec. [Online]. Available: <https://github.com/riscv/riscv-v-spec>
- [6] WebRTC. [Online]. Available: <https://webrtc.org/>
- [7] M. Adler and J.-I. Gailly. Zlib data compression library. [Online]. Available: <https://github.com/madler/zlib>
- [8] S. Aga, S. Jeloka, A. Subramaniyan, S. Narayanasamy, D. Blaauw, and R. Das, "Compute caches," in *2017 IEEE International Symposium on High Performance Computer Architecture (HPCA)*, 2017, pp. 481–492.
- [9] K. Al-Hawaj, O. Afuye, S. Agwa, A. Apsel, and C. Batten, "Towards a reconfigurable bit-serial/bit-parallel vector accelerator using in-situ processing-in-sram," in *2020 IEEE International Symposium on Circuits and Systems (ISCAS)*, 2020, pp. 1–5.
- [10] K. Al-Hawaj, T. Ta, N. Cebry, S. Agwa, O. Afuye, E. Hall, C. Golden, A. B. Apsel, and C. Batten, "Eve: Ephemeral vector engines," in *2023 IEEE International Symposium on High-Performance Computer Architecture (HPCA)*, 2023, pp. 691–704.
- [11] Arm. Arm cortex-a76 core technical reference manual r3p0. [Online]. Available: <https://developer.arm.com/documentation/100798/0300/>
- [12] Arm. Arm optimized routines. [Online]. Available: <https://github.com/ARM-software/optimized-routines>
- [13] Arm. Introducing the scalable matrix extension for the armv9-a architecture. [Online]. Available: <https://community.arm.com/arm-community-blogs/b/architectures-and-processors-blog/posts/scalable-matrix-extension-armv9-a-architecture>
- [14] Arm-Software. Cmsis-dsp, an optimized compute library for embedded systems. [Online]. Available: <https://github.com/ARM-software/CMSIS-DSP>
- [15] I. A. Assir, M. E. Iskandarani, H. R. A. Sandid, and M. A. R. Saghir, "Arrow: A risc-v vector accelerator for machine learning inference," 2021. [Online]. Available: <https://arxiv.org/abs/2107.07169>
- [16] S. K. Bose, V. Mohan, and A. Basu, "A 75kb sram in 65nm cmos for in-memory computing based neuromorphic image denoising," in *2020 IEEE International Symposium on Circuits and Systems (ISCAS)*, 2020, pp. 1–5.
- [17] A. Cabrera, S. Hitefield, J. Kim, S. Lee, N. R. Miniskar, and J. S. Vetter, "Toward performance portable programming for heterogeneous systems on a chip: A case study with qualcomm snapdragon soc," in *2021 IEEE High Performance Extreme Computing Conference (HPEC)*, 2021, pp. 1–7.
- [18] H. Caminal, Y. Chronis, T. Wu, J. M. Patel, and J. F. Martínez, "Accelerating database analytic query workloads using an associative processor," in *Proceedings of the 49th Annual International Symposium on Computer Architecture*, ser. ISCA '22. New York, NY, USA: Association for Computing Machinery, 2022, p. 623–637. [Online]. Available: <https://doi.org/10.1145/3470496.3527435>
- [19] H. Caminal, K. Yang, S. Srinivasa, A. K. Ramanathan, K. Al-Hawaj, T. Wu, V. Narayanan, C. Batten, and J. F. Martínez, "Cape: A content-addressable processing engine," in *2021 IEEE International Symposium on High-Performance Computer Architecture (HPCA)*, 2021, pp. 557–569.
- [20] M. Cavalcante, F. Schuiki, F. Zaruba, M. Schaffner, and L. Benini, "Ara: A 1-ghz+ scalable and energy-efficient risc-v vector processor with multiprecision floating-point support in 22-nm fd-soi," *IEEE Transactions on Very Large Scale Integration (VLSI) Systems*, vol. 28, no. 2, pp. 530–543, 2020.
- [21] M. Cavalcante, F. Schuiki, F. Zaruba, M. Schaffner, and L. Benini, "Ara: A 1-ghz+ scalable and energy-efficient risc-v vector processor with multiprecision floating-point support in 22-nm fd-soi," *IEEE Transactions on Very Large Scale Integration (VLSI) Systems*, vol. 28, no. 2, pp. 530–543, 2020.
- [22] C. Chen, X. Xiang, C. Liu, Y. Shang, R. Guo, D. Liu, Y. Lu, Z. Hao, J. Luo, Z. Chen, C. Li, Y. Pu, J. Meng, X. Yan, Y. Xie, and X. Qi, "Xuantie-910: A commercial multi-core 12-stage pipeline out-of-order 64-bit high performance risc-v processor with vector extension: Industrial product," in *2020 ACM/IEEE 47th Annual International Symposium on Computer Architecture (ISCA)*, 2020, pp. 52–64.
- [23] D. Cheresiz, B. Juurlink, S. Vassiliadis, and H. Wijshoff, "The csi multimedia architecture," *IEEE Transactions on Very Large Scale Integration (VLSI) Systems*, vol. 13, no. 1, pp. 1–13, 2005.
- [24] clMathLibraries. A software library containing sparse functions written in opencl. [Online]. Available: <https://github.com/clMathLibraries/clSPARSE/>
- [25] J. Corbal, R. Espasa, and M. Valero, "Mom: a matrix simd instruction set architecture for multimedia applications," in *SC '99: Proceedings of the 1999 ACM/IEEE Conference on Supercomputing*, 1999, pp. 15–15.
- [26] J. Corbal, R. Espasa, and M. Valero, "Three-dimensional memory vectorization for high bandwidth media memory systems," in *35th Annual IEEE/ACM International Symposium on Microarchitecture, 2002. (MICRO-35). Proceedings.*, 2002, pp. 149–160.
- [27] M. Demler, "Andes plots risc-v vector heading," *Microprocessor Report*, 2020.
- [28] A. Developers. Profile battery usage with batterystats and battery historian. [Online]. Available: <https://developer.android.com/topic/performance/power/setup-battery-historian>
- [29] G. Damos, A. Kerr, S. Yalamanchili, and N. Clark, "Ocelot: A dynamic optimization framework for bulk-synchronous applications in heterogeneous systems," in *2010 19th International Conference on Parallel Architectures and Compilation Techniques (PACT)*, 2010, pp. 353–364.
- [30] J. J. Dongarra, P. Luszczek, and A. Petitet, "The linpack benchmark: past, present and future," *Concurrency and Computation: practice and experience*, vol. 15, no. 9, pp. 803–820, 2003.
- [31] C. Eckert, X. Wang, J. Wang, A. Subramaniyan, D. Sylvester, D. Blaauw, R. Das, and R. Iyer, "Neural cache: Bit-serial in-cache acceleration of deep neural networks," *IEEE Micro*, vol. 39, no. 3, p. 11–19, may 2019. [Online]. Available: <https://doi.org/10.1109/MM.2019.2908101>
- [32] C. N. Fischer and R. J. LeBlanc Jr, *Crafting a Compiler with C*. Benjamin-Cummings Publishing Co., Inc., 1991.
- [33] D. Fujiki, "Mvc: Enabling fully coherent multi-data-views through the memory hierarchy with processing in memory," in *Proceedings of the 56th Annual IEEE/ACM International Symposium on Microarchitecture*, 2023, pp. 800–814.
- [34] D. Fujiki, A. Khadem, S. Mahlke, and R. Das, "Multi-layer in-memory processing," in *2022 55th IEEE/ACM International Symposium on Microarchitecture (MICRO)*, 2022, pp. 920–936.
- [35] D. Fujiki, S. Mahlke, and R. Das, "Duality cache for data parallel acceleration," in *Proceedings of the 46th International Symposium on Computer Architecture*, ser. ISCA '19. New York, NY, USA: Association for Computing Machinery, 2019, p. 397–410. [Online]. Available: <https://doi.org/10.1145/3307650.3322257>
- [36] S. George, M. J. Liao, H. Jiang, J. B. Kotra, M. T. Kandemir, J. Sampson, and V. Narayanan, "Mdacache: Caching for multi-dimensional-access memories," in *2018 51st Annual IEEE/ACM International Symposium on Microarchitecture (MICRO)*, 2018, pp. 841–854.
- [37] Google. Blink (rendering engine). [Online]. Available: <https://www.chromium.org/blink/>
- [38] Google. Boringssl library. [Online]. Available: <https://github.com/google/boringssl>
- [39] Google. Skia - a complete 2d graphic library for drawing text, geometries, and images. [Online]. Available: <https://github.com/google/skia>
- [40] Google. Xnnpack, a highly optimized library of floating-point neural network inference operators. [Online]. Available: <https://github.com/google/XNNPACK>
- [41] gsmarena. Comparing the sizes of flagship chipsets: Qualcomm, samsung, huawei and apple. [Online]. Available: https://www.gsmarena.com/comparing_the_sizes_of_flagship_chipsets_qualcomm_samsung_huawei_adn_apple-news-30240.php
- [42] B. Hawkins, B. Demsky, D. Bruening, and Q. Zhao, "Optimizing binary translation of dynamically generated code," in *Proceedings of the 13th Annual IEEE/ACM International Symposium on Code Generation and Optimization*, ser. CGO '15. USA: IEEE Computer Society, 2015, p. 68–78.
- [43] A. G. Howard, M. Zhu, B. Chen, D. Kalenichenko, W. Wang, T. Weyand, M. Andreetto, and H. Adam, "Mobilenets: Efficient convolutional neural networks for mobile vision applications," 2017. [Online]. Available: <https://arxiv.org/abs/1704.04861>
- [44] T. Instruments. Tms320c5x user's guide. [Online]. Available: <https://www.ti.com/lit/ug/spru056d/spru056d.pdf>
- [45] Intel. Accelerate artificial intelligence (ai) workloads with intel advanced matrix extensions (intel amx). [Online].

- Available: <https://www.intel.com/content/www/us/en/content-details/785250/accelerate-artificial-intelligence-ai-workloads-with-intel-advanced-matrix-extensions-intel-amx.html>
- [46] S. Jeloka, N. B. Akesh, D. Sylvester, and D. Blaauw, "A 28 nm configurable memory (tcam/bcam/sram) using push-rule 6t bit cell enabling logic-in-memory," *IEEE Journal of Solid-State Circuits*, vol. 51, no. 4, pp. 1009–1021, 2016.
- [47] S. Jeloka, N. B. Akesh, D. Sylvester, and D. Blaauw, "A 28 nm configurable memory (tcam/bcam/sram) using push-rule 6t bit cell enabling logic-in-memory," *IEEE Journal of Solid-State Circuits*, vol. 51, no. 4, pp. 1009–1021, 2016.
- [48] M. Kang, E. P. Kim, M.-s. Keel, and N. R. Shanbhag, "Energy-efficient and high throughput sparse distributed memory architecture," in *2015 IEEE International Symposium on Circuits and Systems (ISCAS)*, 2015, pp. 2505–2508.
- [49] A. Khadem, D. Fujiki, N. Talati, S. Mahlke, and R. Das, "Vector-processing for mobile devices: Benchmark and analysis," in *2023 IEEE International Symposium on Workload Characterization (IISWC)*, 2023, pp. 15–27.
- [50] S. Kim, "Reducing area overhead for error-protecting large L2/L3 caches," *IEEE Transactions on Computers*, vol. 58, no. 3, pp. 300–310, 2009.
- [51] Y. Kim, W. Yang, and O. Mutlu, "Ramulator: A fast and extensible dram simulator," *IEEE Computer Architecture Letters*, vol. 15, no. 1, pp. 45–49, 2016.
- [52] K. L. Kloker, "The motorola dsp56000 digital signal processor," *IEEE Micro*, vol. 6, no. 6, pp. 29–48, 1986.
- [53] K. Komatsu, S. Momose, Y. Isobe, O. Watanabe, A. Musa, M. Yokokawa, T. Aoyama, M. Sato, and H. Kobayashi, "Performance evaluation of a vector supercomputer sx-aurora tsubasa," in *SC18: International Conference for High Performance Computing, Networking, Storage and Analysis*, 2018, pp. 685–696.
- [54] M. Kooli, H.-P. Charles, C. Touzet, B. Giraud, and J.-P. Noel, "Smart instruction codes for in-memory computing architectures compatible with standard sram interfaces," in *2018 Design, Automation & Test in Europe Conference & Exhibition (DATE)*, 2018, pp. 1634–1639.
- [55] M. Kooli, A. Heraud, H.-P. Charles, B. Giraud, R. Gauchi, M. Ezzadeen, K. Mambu, V. Egloff, and J.-P. Noel, "Towards a truly integrated vector processing unit for memory-bound applications based on a cost-competitive computational sram design solution," *J. Emerg. Technol. Comput. Syst.*, vol. 18, no. 2, apr 2022. [Online]. Available: <https://doi.org/10.1145/3485823>
- [56] S. Li, N. Xiao, P. Wang, G. Sun, X. Wang, Y. Chen, H. H. Li, J. Cong, and T. Zhang, "Rc-nvm: Dual-addressing non-volatile memory architecture supporting both row and column memory accesses," *IEEE Transactions on Computers*, vol. 68, no. 2, pp. 239–254, 2019.
- [57] libjpeg_turbo. libjpeg-turbo. [Online]. Available: <https://libjpeg-turbo.org/>
- [58] libpng. official png reference library. [Online]. Available: <http://www.libpng.org/pub/png/libpng.html>
- [59] libwebp. Webp codec. [Online]. Available: <https://github.com/webmproject/libwebp>
- [60] B. C. Lopes and R. Auler, *Getting started with LLVM core libraries*. Packt Publishing Ltd, 2014.
- [61] N. Ma, X. Zhang, H.-T. Zheng, and J. Sun, "Shufflenet v2: Practical guidelines for efficient cnn architecture design," 2018. [Online]. Available: <https://arxiv.org/abs/1807.11164>
- [62] F. Minervini and O. Palomar, "Vitruvius: And area-efficient risc-v decoupled vector accelerator for high performance computing," *RISC-V Summit*, 2021.
- [63] F. Minervini, O. Palomar, O. Unsal, E. Reggiani, J. Quiroga, J. Marimon, C. Rojas, R. Figueras, A. Ruiz, A. Gonzalez, J. Mendoza, I. Vargas, C. Hernandez, J. Cabre, L. Khoirunisa, M. Bouhali, J. Pavon, F. Moll, M. Olivieri, M. Kovac, M. Kovac, L. Dragic, M. Valero, and A. Cristal, "Vitruvius+: An area-efficient risc-v decoupled vector coprocessor for high performance computing applications," *ACM Trans. Archit. Code Optim.*, vol. 20, no. 2, mar 2023. [Online]. Available: <https://doi.org/10.1145/3575861>
- [64] N. Muralimanohar, R. Balasubramanian, and N. P. Jouppi, "Cacti 6.0: A tool to model large caches," *HP laboratories*, vol. 27, p. 28, 2009.
- [65] C. Nugteren, "Clblast: A tuned opencl blas library," in *Proceedings of the International Workshop on OpenCL*, ser. IWOCL '18. New York, NY, USA: Association for Computing Machinery, 2018. [Online]. Available: <https://doi.org/10.1145/3204919.3204924>
- [66] Nvidia. Nvidia hopper architecture in-depth. [Online]. Available: <https://developer.nvidia.com/blog/nvidia-hopper-architecture-in-depth/>
- [67] J. S. Olesen. Greedy register allocation in llvm 3.0. [Online]. Available: <http://blog.llvm.org/2011/09/greedy-register-allocation-in-llvm-30.html>
- [68] M. Platzner and P. Puschner, "Vicuna: A Timing-Predictable RISC-V Vector Coprocessor for Scalable Parallel Computation," in *33rd Euromicro Conference on Real-Time Systems (ECRTS 2021)*, ser. Leibniz International Proceedings in Informatics (LIPIcs), B. B. Brandenburg, Ed., vol. 196. Dagstuhl, Germany: Schloss Dagstuhl – Leibniz-Zentrum für Informatik, 2021, pp. 1:1–1:18. [Online]. Available: <https://drops.dagstuhl.de/opus/volltexte/2021/13932>
- [69] qualcomm. Hexagon npu sdk. [Online]. Available: <https://www.qualcomm.com/developer/software/hexagon-npu-sdk>
- [70] Qualcomm. Introducing trepn profiler 6.0. [Online]. Available: <https://developer.qualcomm.com/blog/introducing-trepn-profiler-60>
- [71] Qualcomm. Snapdragon mobile platform opencl general programming and optimization guide. [Online]. Available: <https://developer.qualcomm.com/download/adrenosdk/adreno-opencl-programming-guide.pdf>
- [72] E. Sadredini, R. Rahimi, M. Lenjani, M. Stan, and K. Skadron, "Impala: Algorithm/architecture co-design for in-memory multi-stride pattern matching," in *2020 IEEE International Symposium on High Performance Computer Architecture (HPCA)*, 2020, pp. 86–98.
- [73] E. Sadredini, R. Rahimi, V. Verma, M. Stan, and K. Skadron, "Eap: A scalable and efficient in-memory accelerator for automata processing," in *Proceedings of the 52nd Annual IEEE/ACM International Symposium on Microarchitecture*, ser. MICRO '52. New York, NY, USA: Association for Computing Machinery, 2019, p. 87–99. [Online]. Available: <https://doi.org/10.1145/3352460.3358324>
- [74] M. Sato, Y. Ishikawa, H. Tomita, Y. Kodama, T. Odajima, M. Tsuji, H. Yashiro, M. Aoki, N. Shida, I. Miyoshi, K. Hirai, A. Furuya, A. Asato, K. Morita, and T. Shimizu, "Co-design for a64fx manycore processor and "fugaku"," in *SC20: International Conference for High Performance Computing, Networking, Storage and Analysis*, 2020, pp. 1–15.
- [75] C. Schmidt, J. Wright, Z. Wang, E. Chang, A. Ou, W. Bae, S. Huang, V. Milovanović, A. Flynn, B. Richards *et al.*, "An eight-core 1.44-ghz risc-v vector processor in 16-nm finfet," *IEEE Journal of Solid-State Circuits*, vol. 57, no. 1, pp. 140–152, 2021.
- [76] V. Seshadri, T. Mullins, A. Boroumand, O. Mutlu, P. B. Gibbons, M. A. Kozuch, and T. C. Mowry, "Gather-scatter dram: In-dram address translation to improve the spatial locality of non-unit strided accesses," in *2015 48th Annual IEEE/ACM International Symposium on Microarchitecture (MICRO)*, 2015, pp. 267–280.
- [77] SiFive. Intelligence x280. [Online]. Available: <https://www.sifive.com/document-file/x280-datasheet>
- [78] SiFive. Performance p270. [Online]. Available: <https://www.sifive.com/document-file/x280-datasheet>
- [79] W. A. Simon, Y. M. Qureshi, M. Rios, A. Levisse, M. Zapater, and D. Aienza, "Blade: An in-cache computing architecture for edge devices," *IEEE Transactions on Computers*, vol. 69, no. 9, pp. 1349–1363, 2020.
- [80] N. Stephens, S. Biles, M. Boettcher, J. Eapen, M. Eyole, G. Gabrielli, M. Horsnell, G. Magklis, A. Martinez, N. Premillieu, A. Reid, A. Rico, and P. Walker, "The arm scalable vector extension," *IEEE Micro*, vol. 37, no. 2, pp. 26–39, 2017.
- [81] A. Stillmaker and B. Baas, "Scaling equations for the accurate prediction of cmos device performance from 180nm to 7nm," *Integration*, vol. 58, pp. 74–81, 2017. [Online]. Available: <https://www.sciencedirect.com/science/article/pii/S0167926017300755>
- [82] A. Subramanian, J. Wang, E. R. M. Balasubramanian, D. Blaauw, D. Sylvester, and R. Das, "Cache automaton," in *Proceedings of the 50th Annual IEEE/ACM International Symposium on Microarchitecture*, ser. MICRO-50 '17. New York, NY, USA: Association for Computing Machinery, 2017, p. 259–272. [Online]. Available: <https://doi.org/10.1145/3123939.3123986>
- [83] G. J. Sullivan, J.-R. Ohm, W.-J. Han, and T. Wiegand, "Overview of the high efficiency video coding (hevc) standard," *IEEE Transactions on Circuits and Systems for Video Technology*, vol. 22, no. 12, pp. 1649–1668, 2012.
- [84] T. Ta, K. Al-Hawaj, N. Cebry, Y. Ou, E. Hall, C. Golden, and C. Batten, "big.vllite: On-demand data-parallel acceleration for mobile systems on chip," in *2022 55th IEEE/ACM International Symposium on Microarchitecture (MICRO)*, 2022, pp. 181–198.

- [85] D. Talla, L. John, and D. Burger, "Bottlenecks in multimedia processing with simd style extensions and architectural enhancements," *IEEE Transactions on Computers*, vol. 52, no. 8, pp. 1015–1031, 2003.
- [86] M. Viitanen, A. Koivula, A. Lemmetti, A. Ylä-Outinen, J. Vanne, and T. D. Hämmäläinen, "Kvazaar: Open-source hevc/h.265 encoder," in *Proceedings of the 24th ACM International Conference on Multimedia*, ser. MM '16. New York, NY, USA: Association for Computing Machinery, 2016, p. 1179–1182. [Online]. Available: <https://doi.org/10.1145/2964284.2973796>
- [87] X. Wang, J. Yu, C. Augustine, R. Iyer, and R. Das, "Bit prudent in-cache acceleration of deep convolutional neural networks," in *2019 IEEE International Symposium on High Performance Computer Architecture (HPCA)*, 2019, pp. 81–93.
- [88] S. Wong, C. C. Tamarit, and J. F. Martínez, "Pumice: Processing-using-memory integration with a scalar pipeline for symbiotic execution," in *Design Automation Conference (DAC)*, july 2023.
- [89] J. Zhang, H. Naghibijouybari, and E. Sadredini, "Sealer: In-sram aes for high-performance and low-overhead memory encryption," in *Proceedings of the ACM/IEEE International Symposium on Low Power Electronics and Design*, ser. ISLPED '22. New York, NY, USA: Association for Computing Machinery, 2022. [Online]. Available: <https://doi.org/10.1145/3531437.3539699>